ACS APPLIED MATERIALS & INTERFACES

Research Article

Cite This: ACS Appl. Mater. Interfaces 2018, 10, 19626−19632

www.acsami.org

ZnSe Microsphere/Multiwalled Carbon Nanotube Composites as High-Rate and Long-Life Anodes for Sodium-Ion Batteries

Chunjuan Tang,[†,‡] Xiujuan Wei,[†] Xinyin Cai,[†] Qinyou An,[†] Ping Hu,[†] Jinzhi Sheng,[†] Jiexin Zhu,[†] Shulei Chou,[§] Liming Wu,*[,†] and Liqiang Mai*[,†]

[†]State Key Laboratory of Advanced Technology for Materials Synthesis and Processing, Wuhan University of Technology, Luoshi Road 122, Wuhan 430070, P. R. China

[‡]Department of Mathematics and Physics, Luoyang Institute of Science and Technology, Luoyang 471023, P. R. China

[§]Institute for Superconducting and Electronic Materials, University of Wollongong, Innovation Campus Squires Way, North Wollongong, New South Wales 2522, Australia

Supporting Information

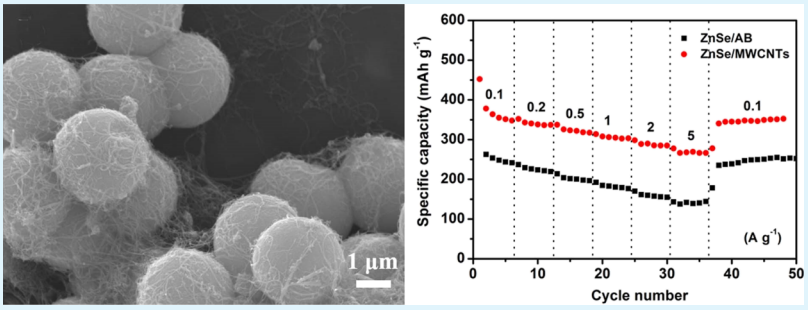

ABSTRACT: Sodium-ion batteries (SIBs) are considered as one of the most favorable alternative devices for sustainable development of modern society. However, it is still a big challenge to search for proper anode materials which have excellent cycling and rate performance. Here, zinc selenide microsphere and multiwalled carbon nanotube (ZnSe/MWCNT) composites are prepared via hydrothermal reaction and following grinding process. The performance of ZnSe/MWCNT composites as a SIB anode is studied for the first time. As a result, ZnSe/MWCNTs exhibit excellent rate capacity and superior cycling life. The capacity retains as high as 382 mA h g^{-1} after 180 cycles even at a current density of 0.5 A g^{-1}. The initial Coulombic efficiency of ZnSe/MWCNTs can reach 88% and nearby 100% in the following cycles. The superior electrochemical properties are attributed to continuous electron transport pathway, improved electrical conductivity, and excellent stress relaxation.

KEYWORDS: *ZnSe microspheres, multiwalled carbon nanotubes, sodium-ion batteries, high-rate, long-life*

INTRODUCTION

With the pollution of environment and the exhaustion of natural resources, the green and more efficient energy storage systems are urgently demanded. Among all kinds of energy storage devices, lithium-ion batteries (LIBs) are the most successful one, which have been widely used in various fields.[1−5] However, the lithium source is very poor in earth, which limits the large-scale application of LIBs. Sodium, whose physical and chemical properties are similar to those of lithium, is considered to be a promising candidate to substitute lithium because of its moderate price and high abundance. However, the relatively larger radius of Na^+ compared with Li^+ causes a larger volume change and poorer cycling stability of electrodes.[6−9] Thus, searching for an electrode material with superior rate performance and cyclic stability is still a major challenge for sodium-ion batteries (SIBs).

Many metal selenides and sulfides are explored as electrode materials for LIBs and SIBs because they are environmentally benign as well as delivering high capacity, such as $SnSe_2$,[10,11] $FeSe_2$,[12−15] $NiSe_2$,[16] $CoSe_2$,[17−20] $MoSe_2$,[21] CoS,[22] and FeS.[23] However, these materials suffer from poor electrochemical properties, which is ascribed to their sluggish kinetics and large volume variations during charge−discharge processes. To circumvent these problems, designing a hierarchical structure[15−19,21] and compositing transition-metal chalcogenides with carbon-based materials[10,13,14,22−25] have been proven to be effective strategies. It is known that the nanostructure facilitates good electrochemical performance; however, the nanoparticles are easy to aggregate. Hierarchically structured materials assembled with nanostructures are porous, which can prevent nanoparticulates from self-aggregating, as well as relieve the stress caused by the repeated charge−discharge process.[26,27] For instance, Zhang et al. synthesized hierarchical $FeSe_2$ microspheres composed of numerous nanooctahedra, exhibit-

Received: February 15, 2018
Accepted: May 14, 2018
Published: May 14, 2018

DOI: 10.1021/acsami.8b02819
ACS Appl. Mater. Interfaces 2018, 10, 19626−19632

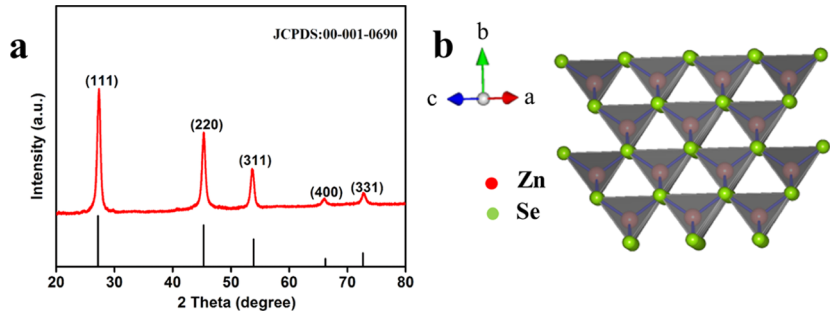

Figure 1. (a) XRD pattern of the obtained ZnSe microspheres and (b) crystal structure of ZnSe.

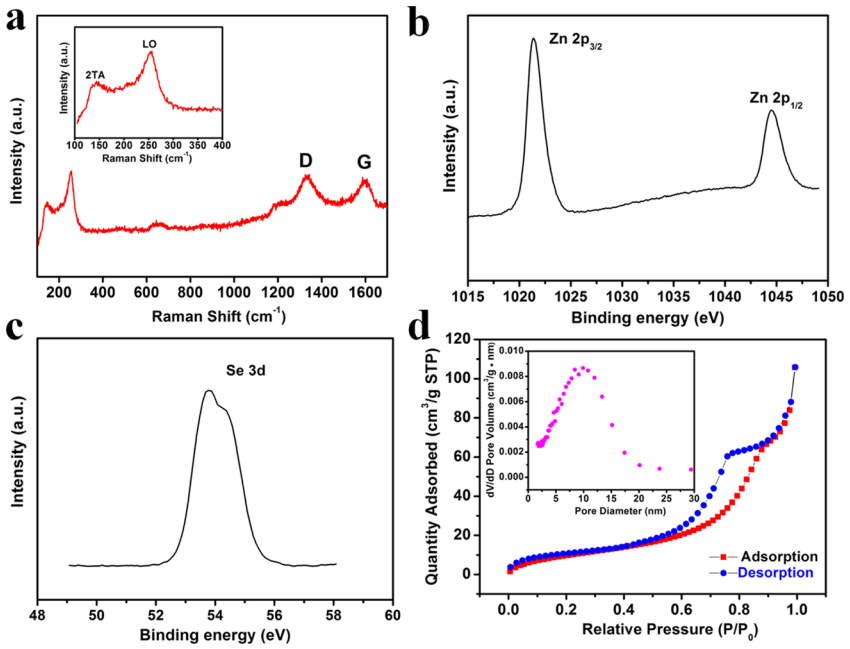

Figure 2. Structural characterization of ZnSe/MWCNTs: (a) Raman spectrum; (b) XPS spectrum of the Zn 2p peak; (c) XPS spectrum of the Se 3d peak; and (d) N_2 sorption isotherms and pore size distribution (inset).

ing superordinary sodium storage capability.[15] Zhu and his co-partners prepared FeS nanodots embedded in carbon nanowires by the combination of an electrospinning technique and a biomolecular (L-cysteine)-assisted hydrothermal method, showing a distinct reversibility.[23] Now, ZnSe is widely used in photodetectors,[28] solar cells,[29] biomedical labels,[30] and photocatalyst.[31,32] In addition, ZnSe also exhibits electrochemical activity as an anode material for LIBs.[33−36] It has been reported that the ZnSe−rGO composites deliver a specific capacity as high as 778 mA h g^{-1} at 1000 mA g^{-1} after 400 cycles.[36] These results indicate that ZnSe is a potential electrode material because of its relatively higher capacity compared with commercial graphite. Therefore, it is worth investigating the sodium storage performance of ZnSe microspheres.

In this paper, we report for the first time a uniform microsized ZnSe spheres composed of primary nanoparticles mixed with multiwalled carbon nanotubes (MWCNTs) which are adopted as an effective conductive network. The ZnSe/MWCNT composites exhibit obviously better electrochemical performance than that of ZnSe/acetylene black (AB) as SIB anode materials. The ZnSe/MWCNT composites deliver a capacity as high as 382 mA h g^{-1} after 180 cycles at 0.5 A g^{-1}, corresponding to a capacity retention of 94% (compared to the second cycle capacity). Quantitative kinetics analysis revealed that the sodium storage performance of ZnSe/MWCNTs is mainly dominated by the diffusion behavior. The initial Coulombic efficiency of ZnSe/MWCNTs can reach 88% and nearby 100% in the following cycles, making it a favorite candidate for the SIB anode material.

RESULTS AND DISCUSSION

The X-ray diffraction (XRD) pattern of ZnSe microspheres (Figure 1a) displays that the diffraction peaks are in accordance with the standard JCPDS no. 00-001-0690. The crystal structure corresponds to $F\bar{4}3m$ space group cubic ZnSe. The average crystallite sizes of the ZnSe nanoparticles are calculated by Scherrer equation, which is determined to be 11.79 nm. Figure 1b reveals the schematic crystal structure of ZnSe, indicating that Zn atoms coordinate with four Se atoms to form the pyramidal [$ZnSe_4$] units. The pyramidal [$ZnSe_4$] units connect with each other through sharing chains.

Figure 2a manifests the Raman spectrum of ZnSe/MWCNTs. It shows four peaks at 141, 253, 1337, and 1598 cm^{-1}. The signals at 141 and 253 cm^{-1} are in well agreement with the 2TA and LO modes of ZnSe,[37] respectively, whereas the MWCNTs show two characteristic peaks at the area of 1337 and 1598 cm^{-1}, which can be ascribed to the D- and G-bands.[38] X-ray photoelectron spectroscopy (XPS) measure-

DOI: 10.1021/acsami.8b02819
ACS Appl. Mater. Interfaces 2018, 10, 19626−19632

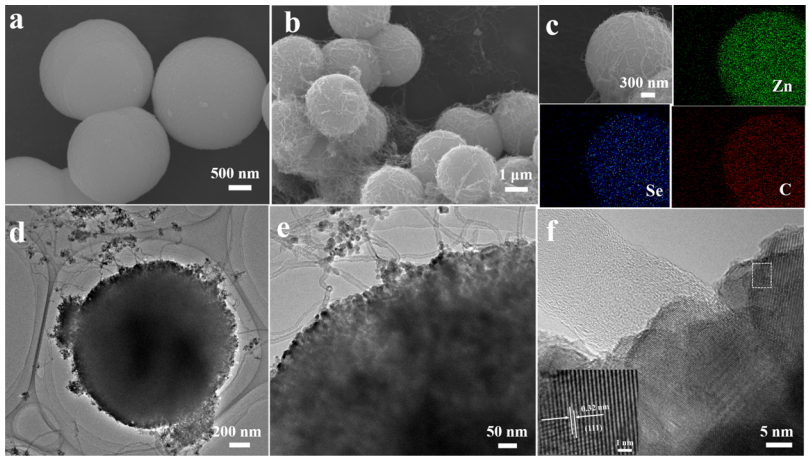

Figure 3. (a) FESEM image of ZnSe microspheres; (b) FESEM image of ZnSe/MWCNTs; (c) EDS mapping images of ZnSe/MWCNTs; (d,e) TEM images of ZnSe/MWCNTs; and (f) HRTEM image of ZnSe/MWCNTs.

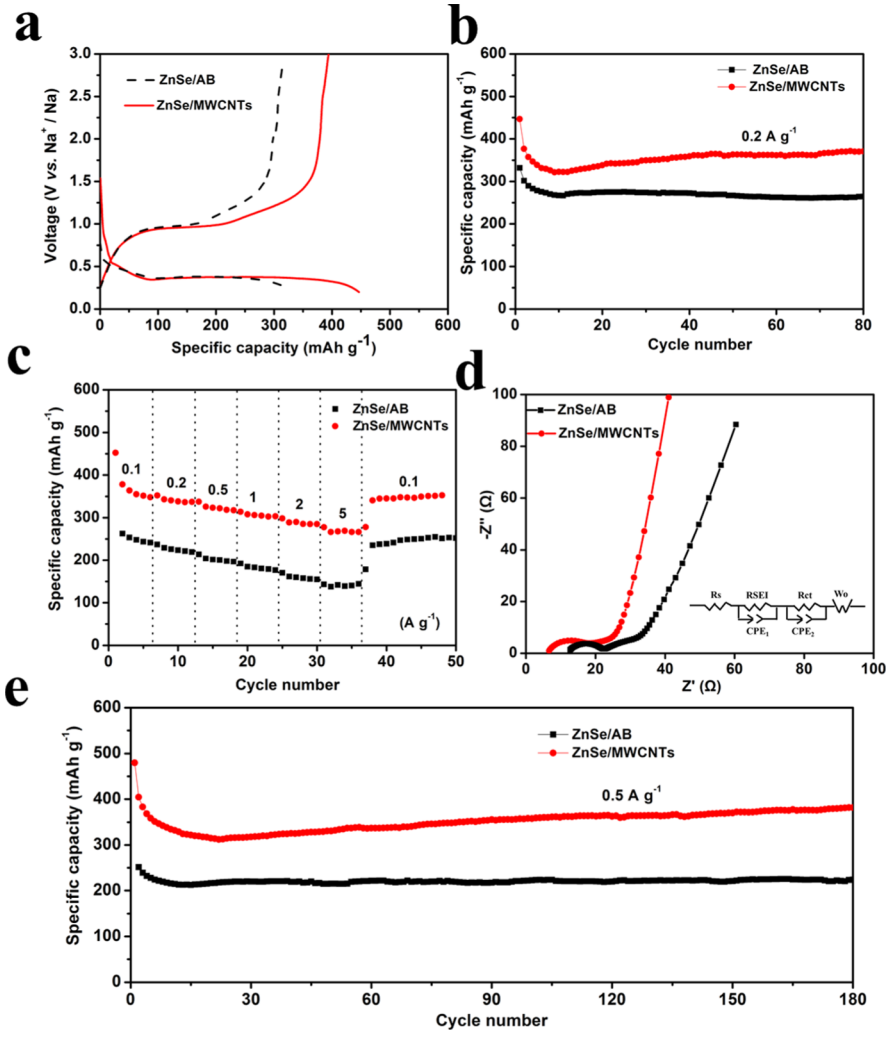

Figure 4. Electrochemical performance of ZnSe/MWCNTs and ZnSe/AB electrodes for SIBs: (a) initial galvanostatic cycling curves at a current density of 0.2 A g^{-1}; (b) cycling performance at 0.2 A g^{-1}; (c) rate performance in the current range of 0.1−5 A g^{-1}; (d) Nyquist plots for ZnSe/MWCNTs and ZnSe/AB electrodes; and (e) long-life cycling performance of ZnSe/MWCNTs and ZnSe/AB electrodes at 0.5 A g^{-1}.

ment was conducted to further confirm the components of ZnSe/MWCNTs. Figure 2b,c shows the XPS spectra obtained from Zn and Se regions of ZnSe/MWCNTs. The signals located at 1021, 1044, and 54 eV can be ascribed to Zn $2p_{3/2}$, Zn $2p_{1/2}$, and Se 3d, respectively.[39] This confirms that the as-prepared samples consist of pure ZnSe with no impurities. The porosity of ZnSe microspheres is analyzed with the N_2 adsorption and desorption analyses (Figure 2d). The specific

DOI: 10.1021/acsami.8b02819
ACS Appl. Mater. Interfaces 2018, 10, 19626−19632

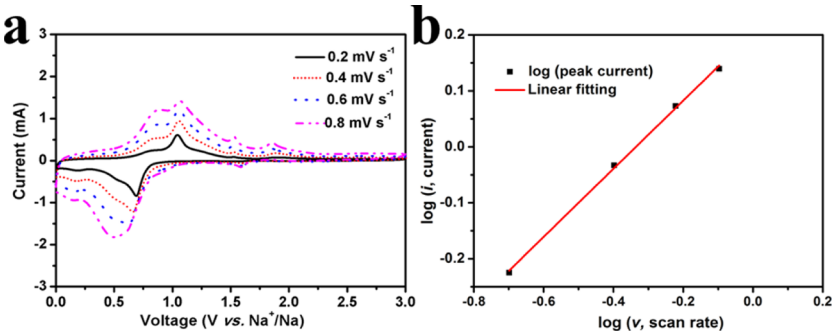

Figure 5. (a) CV profiles of ZnSe/MWCNTs at various scan rates after five cycles and (b) log(i) vs log(v) plot for ZnSe/MWCNTs obtained from the CV data.

BET surface area is determined at a value of 39.3 m^2 g^{-1}, and the Barrett–Joyner–Halenda adsorption pore volume is 0.159 cm^3 g^{-1}. The pore size distribution is mainly in the range of 2–30 nm, centered at about 12 nm (the inset of Figure 2d).

The morphological studies of ZnSe microspheres and ZnSe/MWCNT composites are characterized by field emission scanning electron microscopy (FESEM), transmission electron microscopy (TEM), and high-resolution transmission electron microscopy (HRTEM) (Figure 3). Figure 3a presents the FESEM image of ZnSe microspheres. It can be observed that the ZnSe microspheres are very uniform (about 2 μm) and in a narrow-sized distribution. Because of the tubular shape of MWCNTs, they can form an interconnected electronically conductive network between single ZnSe microspheres, which can guarantee efficient and fast electron transportation (Figure 3b). Energy-dispersive system (EDS) mapping images of ZnSe/MWCNTs indicate the homogeneous distribution of zinc (Zn), selenium (Se), and C in the obtained product (Figure 3c). The elemental mapping images of ZnSe/AB are also tested, as shown in Figure S1. The TEM images displayed in Figure 3d,e further manifest the microstructure of ZnSe/MWCNTs. It reveals that ZnSe microspheres are composed of nanoparticles and possess a porous architecture. The HRTEM image of ZnSe/MWCNTs (Figure 3f) displays that the lattice distance is about 0.32 nm, corresponding to the (111) crystal plane of ZnSe.

The electrochemical performances of ZnSe/MWCNT and ZnSe/AB samples are investigated by assembling the half-cells. The cyclic voltammetry (CV) curves of ZnSe/MWCNT electrodes are recorded between 0.01 and 3.0 V (Figure S2). The initial curve shows an obvious cathodic peak at 0.24 V and an anodic peak at 0.99 V. The sharp cathodic peak is ascribed to the conversion from ZnSe to metal/Na_2Se and the formation of SEI layer on the electrode,[36,40] whereas the anodic peak can be ascribed to the transformation reaction from metal to metal selenides on the electrode. In the following cycles, the cathodic peak is shifted to higher potential, which is attributed to the structure and volume change resulting from the conversion reaction, whereas the following CV curves are overlapped well, indicating an excellent cycle reversibility of electrodes.

The initial cycling profiles of ZnSe/MWCNT and ZnSe/AB electrodes at 0.2 A g^{-1} are presented in Figure 4a. Both samples show similar low discharge plateaus at around 0.3 V and similar charge plateaus at around 1.0 V, which corresponds well to the redox peaks in CV graphs. The ZnSe/MWCNT electrode delivers a first discharge capacity of 447 mA h g^{-1}, a much higher value than that of ZnSe/AB, to be specific, only 332 mA h g^{-1}. Figure S3 describes the cycling curves of ZnSe/MWCNT and ZnSe/AB electrodes after 80 cycles, which show similar appearance, indicating an identical electrochemical reaction of ZnSe in both composites. Figure 4b presents electrochemical performance of ZnSe/MWCNT and ZnSe/AB electrodes. The capacity retentions of ZnSe/MWCNT and ZnSe/AB electrodes after 80 cycles are 83 and 79%, respectively. Compared with ZnSe/AB electrodes, ZnSe/MWCNT electrodes show better electrochemical performance, delivering relatively high capacity. It is noted that in the initial few cycles, the capacity of ZnSe/MWCNT electrode decreases. Then, the capacity increases slowly and finally stabilizes at a value of about 362 mA h g^{-1}. The increased capacity can be attributed to the reactivation of ZnSe/MWCNT microspheres.[5,41] The reactivation of the electrode can lead to more defects and active site formation, facilitating the sodium storage.[36]

The rate performances of ZnSe/MWCNT and ZnSe/AB samples are tested in the range of 0.1–5 A g^{-1} (Figure 4c). The discharge capacities of ZnSe/MWCNTs are 370, 350, 324, 313, 288, and 271 mA h g^{-1} at different rates of 0.1, 0.2, 0.5, 1, 2, and 5 A g^{-1}, respectively. When the rate recovers to 0.1 A g^{-1}, the discharge capacity of ZnSe/MWCNTs can still reach 352 mA h g^{-1}. It can be obviously observed that the rate performances of ZnSe/AB are inferior to that of ZnSe/MWCNTs. Figure S4 displays the cycling plots of ZnSe/MWCNTs at various rates in accordance with Figure 4c. It shows stable charge–discharge curves, indicating excellent rate performance of ZnSe/MWCNTs. The above results demonstrate that the ZnSe/MWCNT electrodes have better cycling capacity and rate performance than ZnSe/AB electrodes. It is reported that the surface area of MWCNTs can significantly affect the enhancement of the rate capabilities and electrochemical performances.[42,43]

To gain insights of the factors that enhance the electrochemical performance of ZnSe/MWCNTs, the electrochemical impedance spectra are measured (Figure 4d). The Nyquist plots show that the electrolyte and cell component resistance (R_s), the solid electrolyte interface (R_{SEI}), and charge-transfer resistance (R_{ct}) of the as-prepared ZnSe/MWCNTs are smaller than those of ZnSe/AB (Table S1). This demonstrates the faster kinetics of the as-prepared ZnSe/MWCNTs, facilitating the electrode to enhance electrochemical performance.

Figure 4e demonstrates the long-life cycling performances of ZnSe/MWCNTs and ZnSe/AB at 0.5 A g^{-1}. The first and second cycle capacities of the ZnSe/MWCNT electrode are 480 and 405 mA h g^{-1}, respectively. Even after 180 cycles, the capacity of the ZnSe/MWCNT electrode can still reach 382 mA h g^{-1}. The capacity retention is 94% compared to the second cycle capacity. However, after cycling the same cycles,

DOI: 10.1021/acsami.8b02819
ACS Appl. Mater. Interfaces 2018, 10, 19626–19632

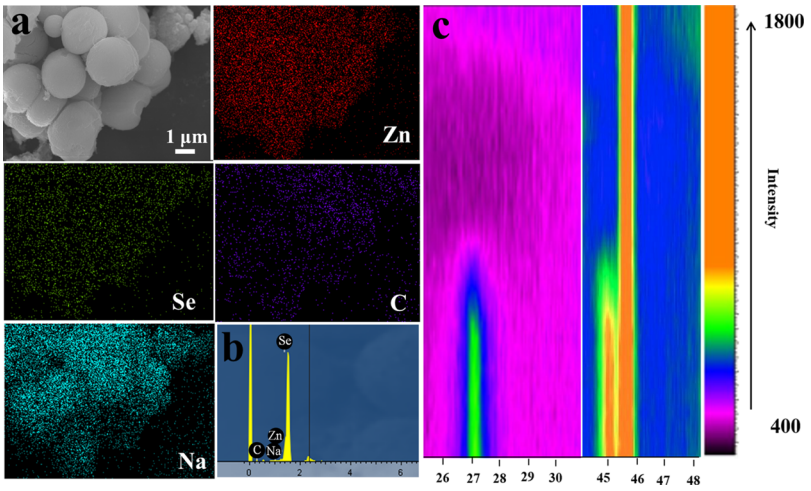

Figure 6. (a,b) EDS mapping images and spectrum of ZnSe/MWCNTs after 100 cycles, respectively and (c) in situ XRD patterns recorded during galvanostatic cycling of the ZnSe/MWCNT electrode.

the ZnSe/AB electrode can only deliver a low capacity of only 224 mA h g^{-1}. In addition, the initial and second Coulombic efficiencies of ZnSe/MWCNTs are about 88, 96%, and nearby 100% in the following cycles (Figure S5), making it a favorite candidate for SIB anode material.

To evaluate the electrochemical kinetics of ZnSe/MWCNTs, CV profiles of ZnSe/MWCNTs tested with various scan rates are displayed in Figure 5a (0.2−0.8 mV s^{-1}). On the basis of the correlation of peak current (i) and the scan rate (v)[44]

$$i = av^b$$

In which i refers to the peak current, v represents the scan rate, a and b are parameters that can be adjusted. The b value indicates the type of Na^+ insertion/extraction, which is settled by the slope of $\log(v)-\log(i)$ plots. When the b value is 0.5, the current is precisely in proportion to the scan rate square root, indicating the diffusion-controlled behavior. For the b value of 1.0, the electrochemical reaction can be mainly ascribed to pseudocapacitive capacity. For the oxidation peak at 1.05 V, $\log(v)$ is linearly related to $\log(i)$ plots (Figure 5b). The b value is 0.61, which is close to 0.5. It demonstrates that the capacity of ZnSe/MWCNTs is mainly contributed by the ionic diffusion behavior.

To further explain the excellent electrochemical performance of the ZnSe/MWCNT electrode, the elemental mappings (Figure 6a) and EDS pattern (Figure 6b) of the ZnSe/MWCNT electrode after 100 cycles are characterized. In addition, the SEM images of ZnSe/AB after 100 cycles are depicted in Figure S6. It is observed that the morphologies of ZnSe microspheres in both composites can be well-preserved after sodium-ion insertion. The results demonstrate that the porous structure can suppress the volume variation of ZnSe microspheres caused by repeating insertion/extraction of Na^+, enhancing the cycling stability of ZnSe microspheres. For the first time, in situ XRD was employed to explore the Na^+ storage mechanisms of ZnSe/MWCNTs. The in situ experiment was conducted at room temperature, and the structural transformation is depicted in Figure 6c. During the initial sodiation process, the peaks at 27° and 45° are well-consistent with (111) and (220) planes of ZnSe, respectively. Proceeding the electrochemical reaction, the typical peaks weaken slowly and finally disappear. The above results demonstrate that sodium-ion insertion induces the amorphization of the ZnSe electrode during the charge−discharge process. The similar phenomenon also occurs in other anode materials.[45,46]

On the basis of the aforementioned results, the superior electrochemical properties of ZnSe/MWCNTs are attributed to the cooperation of the porous structure and the continuous conductive network. The porous structure can accommodate the volume variation, provide open channel for sodium ion to insert, and keep the structural stability. The MWCNT conductive network enhances the electron-transfer kinetics. Integrating the advantages of porous microspheres and MWCNT matrix can significantly increase the cycling and rate performance of the ZnSe electrode.

CONCLUSIONS

The ZnSe/MWCNT composites are successfully prepared through hydrothermal reaction and following grinding process. When assessed as the anode electrode material for SIBs, it manifests superior rate capability and long cycling life. In particular, the ZnSe/MWCNT electrode can still retain the capacity as high as 382 mA h g^{-1} after 180 cycles at a current density of 0.5 A g^{-1}. The initial Coulombic efficiency of ZnSe/MWCNTs can reach 88% and nearby 100% in the following cycles, enabling it a good candidate for SIB anode material. The predominant electrochemical performance of ZnSe/MWCNT composites is ascribed to continuous electron transport pathway, enhanced electrical conductivity, and excellent stress relaxation.

ASSOCIATED CONTENT

Supporting Information

The Supporting Information is available free of charge on the ACS Publications website at DOI: 10.1021/acsami.8b02819.

Material preparation of ZnSe/MWCNT composites, material characterizations, and electrochemical measurements; EDS mapping images of ZnSe/AB; CV plots of ZnSe/MWCNTs at a scan rate of 0.1 mV s^{-1}; the charge−discharge curves of as-prepared ZnSe/MWCNTs and ZnSe/AB electrodes after 80 cycles at 0.2 A g^{-1}; the charge−discharge profiles of ZnSe/MWCNTs at different rates; Coulombic efficiency of ZnSe/MWCNTs at a high current density of 0.5 A g^{-1};

DOI: 10.1021/acsami.8b02819
ACS Appl. Mater. Interfaces 2018, 10, 19626−19632

SEM images of as-prepared ZnSe/AB after 100 cycles; and fitted resistance values of EIS results (PDF)

AUTHOR INFORMATION

Corresponding Authors

*E-mail: liming_wu@whut.edu.cn (L.W.).
*E-mail: mlq518@whut.edu.cn (L.M.).

ORCID

Shulei Chou: 0000-0003-1155-6082
Liqiang Mai: 0000-0003-4259-7725

Author Contributions

Authors C. Tang, X. Wei, and X. Cai make the same contribution to this work. The manuscript has been revised by all authors. All authors have given approval to the final version of the manuscript.

Notes

The authors declare no competing financial interest.

ACKNOWLEDGMENTS

The work was financially supported by the following fundings. Author L. Mai received fundings from the National Natural Science Fund for Distinguished Young Scholars (51425204), National Key Research and Development Program of China (2016YFA0202603), and the National Natural Science Foundation of China (51521001). Author Q. An received fundings from the National Natural Science Foundation of China (51602239), the Hubei Provincial Natural Science Foundation (2016CFB267), and the Fundamental Research Funds for the Central Universities (2016IVA090 and 2017III005). Author C. Tang received fundings from the Henan Provincial Natural Science Foundation (182102410100), the Education Department of Henan Province (17A430004 and 16A140012), and the China Postdoctoral Science Foundation (2016M592401). Author L. Wu received funding from the Fundamental Research Funds for the Central Universities (2017III006).

REFERENCES

(1) Poizot, P.; Laruelle, S.; Grugeon, S.; Dupont, L.; Tarascon, J. M. Nano-Sized Transition-Metal Oxides as Negative-Electrode Materials for Lithium-Ion Batteries. *Nature* **2000**, *407*, 496−499.

(2) Zhang, W.-M.; Wu, X.-L.; Hu, J.-S.; Guo, Y.-G.; Wan, L.-J. Carbon Coated Fe_3O_4 Nanospindles as a Superior Anode Material for Lithium-Ion Batteries. *Adv. Funct. Mater.* **2008**, *18*, 3941−3946.

(3) Wang, N.; Xu, H.; Chen, L.; Gu, X.; Yang, J.; Qian, Y. A General Approach for MFe_2O_4 (M= Zn, Co, Ni) Nanorods and Their High Performance as Anode Materials for Lithium Ion Batteries. *J. Power Sources* **2014**, *247*, 163−169.

(4) Zhao, Y.; Li, X.; Yan, B.; Li, D.; Lawes, S.; Sun, X. Significant Impact of 2D Graphene Nanosheets on Large Volume Change Tin-Based Anodes in Lithium-Ion Batteries: a Review. *J. Power Sources* **2015**, *274*, 869−884.

(5) Wei, X.; Tang, C.; Wang, X.; Zhou, L.; Wei, Q.; Yan, M.; Sheng, J.; Hu, P.; Wang, B.; Mai, L. Copper Silicate Hydrate Hollow Spheres Constructed by Nanotubes Encapsulated in Reduced Graphene Oxide as Long-Life Lithium-Ion Battery Anode. *ACS Appl. Mater. Interfaces* **2015**, *7*, 26572−26578.

(6) Yan, Y.; Yin, Y.-X.; Guo, Y.-G.; Wan, L.-J. A Sandwich-Like Hierarchically Porous Carbon/Graphene Composite as a High-Performance Anode Material for Sodium-Ion Batteries. *Adv. Energy Mater.* **2014**, *4*, 1301584.

(7) Xu, Y.; Zhu, Y.; Liu, Y.; Wang, C. Electrochemical Performance of Porous Carbon/Tin Composite Anodes for Sodium-Ion and Lithium-Ion Batteries. *Adv. Energy Mater.* **2013**, *3*, 128−133.

(8) Zhu, H.; Jia, Z.; Chen, Y.; Weadock, N.; Wan, J.; Vaaland, O.; Han, X.; Li, T.; Hu, L. Tin Anode for Sodium-Ion Batteries using Natural Wood Fiber as a Mechanical Buffer and Electrolyte Reservoir. *Nano Lett.* **2013**, *13*, 3093−3100.

(9) Bommier, C.; Luo, W.; Gao, W.-Y.; Greaney, A.; Ma, S.; Ji, X. Predicting Capacity of Hard Carbon Anodes in Sodium-Ion Batteries using Porosity Measurements. *Carbon* **2014**, *76*, 165−174.

(10) Choi, J.; Jin, J.; Jung, I. G.; Kim, J. M.; Kim, H. J.; Son, S. U. $SnSe_2$ Nanoplate-Graphene Composites as Anode Materials for Lithium Ion Batteries. *Chem. Commun.* **2011**, *47*, 5241−5243.

(11) Zhang, F.; Xia, C.; Zhu, J.; Ahmed, B.; Liang, H.; Velusamy, D. B.; Schwingenschlögl, U.; Alshareef, H. N. $SnSe_2$ 2D Anodes for Advanced Sodium Ion Batteries. *Adv. Energy Mater.* **2016**, *6*, 1601188.

(12) Mai, L. Q.; Gao, Y.; Guan, J. G.; Hu, B.; Xu, L.; Jin, W. Formation and Lithiation of Ferroselite Nanoflowers as High-Energy Li-Ion Battery Electrodes. *Int. J. Electrochem. Sci.* **2009**, *4*, 755−761.

(13) Cho, J. S.; Lee, J.-K.; Kang, Y. C. Graphitic Carbon-Coated $FeSe_2$ Hollow Nanosphere-Decorated Reduced Graphene Oxide Hybrid Nanofibers as an Efficient Anode Material for Sodium Ion Batteries. *Sci. Rep.* **2016**, *6*, 23699.

(14) Zhao, F.; Shen, S.; Cheng, L.; Ma, L.; Zhou, J.; Ye, H.; Han, N.; Wu, T.; Li, Y.; Lu, J. Improved Sodium-Ion Storage Performance of Ultrasmall Iron Selenide Nanoparticles. *Nano Lett.* **2017**, *17*, 4137−4142.

(15) Zhang, K.; Hu, Z.; Liu, X.; Tao, Z.; Chen, J. $FeSe_2$ Microspheres as a High-Performance Anode Material for Na-Ion Batteries. *Adv. Mater.* **2015**, *27*, 3305−3309.

(16) Fan, H.; Yu, H.; Wu, X.; Zhang, Y.; Luo, Z.; Wang, H.; Guo, Y.; Madhavi, S.; Yan, Q. Controllable Preparation of Square Nickel Chalcogenide (NiS and $NiSe_2$) Nanoplates for Superior Li/Na Ion Storage Properties. *ACS Appl. Mater. Interfaces* **2016**, *8*, 25261−25267.

(17) Lu, W.; Xue, M.; Chen, X.; Chen, C. $CoSe_2$ Nanoparticles as Anode for Lithium Ion Battery. *Int. J. Electrochem. Sci.* **2017**, *12*, 1118−1129.

(18) Zhang, K.; Park, M.; Zhou, L.; Lee, G.-H.; Li, W.; Kang, Y.-M.; Chen, J. Urchin-Like $CoSe_2$ as a High-Performance Anode Material for Sodium-Ion Batteries. *Adv. Funct. Mater.* **2016**, *26*, 6728−6735.

(19) Ko, Y. N.; Choi, S. H.; Kang, Y. C. Hollow Cobalt Selenide Microspheres: Synthesis and Application as Anode Materials for Na-Ion Batteries. *ACS Appl. Mater. Interfaces* **2016**, *8*, 6449−6456.

(20) Ali, Z.; Tang, T.; Huang, X.; Wang, Y.; Asif, M.; Hou, Y. Cobalt Selenide Decorated Carbon Spheres for Excellent Cycling Performance of Sodium Ion Batteries. *Energy Storage Mater.* **2018**, *13*, 19−28.

(21) Ko, Y. N.; Choi, S. H.; Park, S. B.; Kang, Y. C. Hierarchical $MoSe_2$ Yolk-Shell Microspheres with Superior Na-Ion Storage Properties. *Nanoscale* **2014**, *6*, 10511−10515.

(22) Wu, R.; Wang, D. P.; Rui, X.; Liu, B.; Zhou, K.; Law, A. W. K.; Yan, Q.; Wei, J.; Chen, Z. In-Situ Formation of Hollow Hybrids Composed of Cobalt Sulfides Embedded within Porous Carbon Polyhedra/Carbon Nanotubes for High-Performance Lithium-Ion Batteries. *Adv. Mater.* **2015**, *27*, 3038−3044.

(23) Zhu, C.; Wen, Y.; van Aken, P. A.; Maier, J.; Yu, Y. High Lithium Storage Performance of FeS Nanodots in Porous Graphitic Carbon Nanowires. *Adv. Funct. Mater.* **2015**, *25*, 2335−2342.

(24) Park, G. D.; Cho, J. S.; Lee, J.-K.; Kang, Y. C. Na-ion Storage Performances of $FeSe_x$ and Fe_2O_3 Hollow Nanoparticles-Decorated Reduced Graphene Oxide Balls prepared by Nanoscale Kirkendall Diffusion Process. *Sci. Rep.* **2016**, *6*, 22432.

(25) Li, H.; Su, Y.; Sun, W.; Wang, Y. Carbon Nanotubes Rooted in Porous Ternary Metal Sulfide@N/S-Doped Carbon Dodecahedron: Bimetal-Organic- Frameworks Derivation and Electrochemical Application for High-Capacity and Long-Life Lithium-Ion Batteries. *Adv. Funct. Mater.* **2016**, *26*, 8345−8353.

(26) Wang, D.; Zhang, G.; Shan, Z.; Zhang, T.; Tian, J. Hierarchically Micro-/Nanostructured TiO_2/Micron Carbon Fibers Composites for Long-Life and Fast-Charging Lithium-Ion Batteries. *ChemElectroChem* **2018**, *5*, 540−545.

(27) Li, F.; Zhou, Z. Micro/Nanostructured Materials for Sodium Ion Batteries and Capacitors. *Small* **2018**, *14*, 1702961.

DOI: 10.1021/acsami.8b02819
ACS Appl. Mater. Interfaces 2018, 10, 19626−19632

(28) Fang, X.; Xiong, S.; Zhai, T.; Bando, Y.; Liao, M.; Gautam, U. K.; Koide, Y.; Zhang, X.; Qian, Y.; Golberg, D. High-Performance Blue/Ultraviolet-Light-Sensitive ZnSe-Nanobelt Photodetectors. *Adv. Mater.* **2009**, *21*, 5016−5021.
(29) Wang, K.; Chen, J.; Zhou, W.; Zhang, Y.; Yan, Y.; Pern, J.; Mascarenhas, A. Direct Growth of Highly Mismatched Type II ZnO/ZnSe Core/Shell Nanowire Arrays on Transparent Conducting Oxide Substrates for Solar Cell Applications. *Adv. Mater.* **2008**, *20*, 3248−3253.
(30) Pradhan, N.; Battaglia, D. M.; Liu, Y.; Peng, X. Efficient, Stable, Small, and Water-Soluble Doped ZnSe Nanocrystal Emitters as Non-Cadmium Biomedical Labels. *Nano Lett.* **2007**, *7*, 312−317.
(31) Cao, F.; Shi, W.; Zhao, L.; Song, S.; Yang, J.; Lei, Y.; Zhang, H. Hydrothermal Synthesis and High Photocatalytic Activity of 3D Wurtzite ZnSe Hierarchical Nanostructures. *J. Phys. Chem. C* **2008**, *112*, 17095−17101.
(32) Wu, Z.; Wang, H.; Xue, Y.; Li, B.; Geng, B. ZnO Nanorods/ZnSe Heteronanostructure Arrays with a Tunable Microstructure of ZnSe Shell for Visible Light Photocatalysis. *J. Mater. Chem. A* **2014**, *2*, 17502−17510.
(33) Fu, Y.; Zhang, Z.; Du, K.; Qu, Y.; Li, Q.; Yang, X. Spherical-like ZnSe with Facile Synthesis as a Potential Electrode Material for Lithium Ion Batteries. *Mater. Lett.* **2015**, *146*, 96−98.
(34) Xu, Y.; Liang, J.; Zhang, K.; Zhu, Y.; Wei, D.; Qian, Y. Origin of Additional Capacities in Selenium-Based ZnSe@C Nanocomposite Li-Ion Battery Electrodes. *Electrochem. Commun.* **2016**, *65*, 44−47.
(35) Kwon, H.-T.; Park, C.-M. Electrochemical Characteristics of ZnSe and its Nanostructured Composite for Rechargeable Li-Ion Batteries. *J. Power Sources* **2014**, *251*, 319−324.
(36) Zhang, Z.; Fu, Y.; Yang, X.; Qu, Y.; Li, Q. Nanostructured ZnSe Anchored on Graphene Nanosheets with Superior Electrochemical Properties for Lithium Ion Batteries. *Electrochim. Acta* **2015**, *168*, 285−291.
(37) Lu, G.; An, H.; Chen, Y.; Huang, J.; Zhang, H.; Xiang, B.; Zhao, Q.; Yu, D.; Du, W. Temperature Dependence of Raman Scattering of ZnSe Nanoparticle Grown through Vapor Phase. *J. Cryst. Growth* **2005**, *274*, 530−535.
(38) Antunes, E. F.; Lobo, A. O.; Corat, E. J.; Trava-Airoldi, V. J.; Martin, A. A.; Veríssimo, C. Comparative Study of First- and Second-Order Raman Spectra of MWCNT at Visible and Infrared Laser Excitation. *Carbon* **2006**, *44*, 2202−2211.
(39) Khawaja, E. E.; Durrani, S. M. A.; Hallak, A. B.; Salim, M. A.; Hussain, M. S. Density of Thin Vapour-Deposited Films of Zinc Selenide. *J. Phys. D: Appl. Phys.* **1994**, *27*, 1008.
(40) Su, D.; Kretschmer, K.; Wang, G. Improved Electrochemical Performance of Na-Ion Batteries in Ether-Based Electrolytes: A Case Study of ZnS Nanospheres. *Adv. Energy Mater.* **2016**, *6*, 1501785.
(41) Sun, H.; Xin, G.; Hu, T.; Yu, M.; Shao, D.; Sun, X.; Lian, J. High-Rate Lithiation-Induced Reactivation of Mesoporous Hollow Spheres for Long-Lived Lithium-Ion Batteries. *Nat. Commun.* **2014**, *5*, 4526.
(42) Xu, D.; Li, B.; Wei, C.; He, Y.-B.; Du, H.; Chu, X.; Qin, X.; Yang, Q.-H.; Kang, F. Preparation and Characterization of MnO_2/acid-treated CNT Nanocomposites for Energy Storage with Zinc Ions. *Electrochim. Acta* **2014**, *133*, 254−261.
(43) Hu, L.; Chen, W.; Xie, X.; Liu, N.; Yang, Y.; Wu, H.; Yao, Y.; Pasta, M.; Alshareef, H. N.; Cui, Y. Symmetrical MnO_2−Carbon Nanotube−Textile Nanostructures for Wearable Pseudocapacitors with High Mass Loading. *ACS Nano* **2011**, *5*, 8904−8913.
(44) Lindström, H.; Södergren, S.; Solbrand, A.; Rensmo, H.; Hjelm, J.; Hagfeldt, A.; Lindquist, S.-E. Li^+ Ion Insertion in TiO_2 (Anatase). 2. Voltammetry on Nanoporous Films. *J. Phys. Chem. B* **1997**, *101*, 7717−7722.
(45) An, Q.; Lv, F.; Liu, Q.; Han, C.; Zhao, K.; Sheng, J.; Wei, Q.; Yan, M.; Mai, L. Amorphous Vanadium Oxide Matrixes Supporting Hierarchical Porous Fe_3O_4/Graphene Nanowires as a High-Rate Lithium Storage Anode. *Nano Lett.* **2014**, *14*, 6250−6256.
(46) Wei, X.; Tang, C.; An, Q.; Yan, M.; Wang, X.; Hu, P.; Cai, X.; Mai, L. $FeSe_2$ Clusters with Excellent Cyclability and Rate Capability for Sodium-Ion Batteries. *Nano Res.* **2017**, *10*, 3202−3211.

DOI: 10.1021/acsami.8b02819
ACS Appl. Mater. Interfaces 2018, 10, 19626−19632